APOE suppresses osteosarcoma by modulating ferroptosis through the mTOR/Stat3 signaling pathway

Keywords
Autophagy, Ferroptosis, Osteosarcoma, APOE, mTOR/Stat3 signaling pathway

Abstract

Introduction

Osteosarcoma (OS) is a highly malignant bone tumor with limited treatment options. The role of Apolipoprotein E (APOE) in OS remains unclear. This study explores the impact of APOE overexpression on OS, particularly its effects on ferroptosis and autophagy.

Material and methods

APOE was identified as a key gene through weighted gene co-expression network analysis (WGCNA) and protein-protein interaction (PPI) network analysis of the GSE28424 dataset. APOE was overexpressed in OS cell lines to evaluate its effects on cell behavior. The role of autophagy was investigated using the autophagy inhibitor 3-MA. The involvement of ferroptosis and the mTOR/Stat3 signaling pathway was investigated utilizing Quantitative real-time reverse transcription PCR (qRT-PCR), Western blot (WB), and flow cytometry. A mouse xenograft model was employed to validate the in vitro results.

Results

APOE overexpression significantly inhibited OS cell proliferation, invasion, migration, and epithelial-mesenchymal transition (EMT), with 3-MA partially reversing these effects. APOE overexpression also inhibited the mTOR and Stat3 expression, enhancing autophagy, as shown by increased LC3B-1, LC3B-2, and Beclin1 expression. Additionally, APOE overexpression promoted apoptosis, associated with increased reactive oxygen species (ROS) and intracellular Fe^{2} levels, and altered ferroptosis-related gene expression, including upregulation of TfR1 and downregulation of FPN, GPX4, and SLC7A11. In vivo, APOE overexpression in a mouse xenograft model resulted in significantly smaller tumors, with changes in autophagy and ferroptosis markers consistent with in vitro findings.

Conclusions

APOE overexpression suppresses osteosarcoma growth by promoting ferroptosis and autophagy through the mTOR/Stat3 signaling pathway, highlighting its promise as a target for OS therapeutic intervention.

APOE suppresses osteosarcoma by modulating ferroptosis through the mTOR/Stat3 signaling pathway

Xiangyang Cheng[#], Chong Bian[#], Yiming Zhang, Huijie Gu, Guangnan Chen, Liang Wu*

Department of Orthopedics, Minhang Hospital, Fudan University, No. 170 Xinsong Road, Minhang District, Shanghai, 201199, China.

[#]**These authors contributed equally.**

*Corresponding author

Liang Wu, Mr

Email: wuliang7860@163.com

Department of Orthopedics, Minhang Hospital, Fudan University, No. 170 Xinsong Road, Minhang District, Shanghai, 201199, China.

Abstract:

Background:

Osteosarcoma (OS) is a highly malignant bone tumor with limited treatment options. The role of Apolipoprotein E (*APOE*) in OS remains unclear. This study explores the impact of *APOE* overexpression on OS, particularly its effects on ferroptosis and autophagy.

Methods:

APOE was identified as a key gene through weighted gene co-expression network analysis (WGCNA) and protein-protein interaction (PPI) network analysis of the GSE28424 dataset. *APOE* was overexpressed in OS cell lines to evaluate its effects on cell behavior. The role of autophagy was investigated using the autophagy inhibitor 3-methyladenine (3-MA). The involvement of ferroptosis and the mTOR/Stat3 signaling pathway was investigated utilizing Quantitative real-time reverse transcription PCR (qRT-PCR), Western blot (WB), and flow cytometry. A mouse xenograft model was employed to validate the in vitro results.

Results:

APOE overexpression significantly inhibited OS cell proliferation, invasion, migration, and epithelial-mesenchymal transition (EMT), with 3-MA partially reversing these effects. *APOE* overexpression also inhibited the mTOR and Stat3 expression, enhancing autophagy, as shown by increased LC3B-1, LC3B-2, and Beclin1 expression. Additionally, *APOE* overexpression promoted apoptosis, associated with increased reactive oxygen species (ROS) and intracellular Fe^{2+} levels, and altered ferroptosis-related gene expression, including upregulation of *TfR1* and downregulation of *FPN*, *GPX4*, and *SLC7A11*. *In vivo*, *APOE* overexpression in a mouse xenograft model resulted in significantly smaller tumors, with changes in autophagy and ferroptosis markers consistent with *in vitro* findings.

Conclusion:

APOE overexpression suppresses osteosarcoma growth by promoting ferroptosis and autophagy through the mTOR/Stat3 signaling pathway, highlighting its promise as a target for OS therapeutic intervention.

Keywords: Osteosarcoma, *APOE*, Ferroptosis, mTOR/Stat3 signaling pathway, Autophagy

Running title: *APOE* inhibits OS via ferroptosis and mTOR/Stat3

Introduction

Osteosarcoma (OS) is a primary malignant bone cancer is a primary malignant bone tumor defined by tumor cells directly forming osteoid tissue, with an incidence of approximately 3.4 cases per million individuals annually(1). Predominantly affecting young people, teenagers, and youngsters between the ages of 10 and 25, OS exhibits a higher incidence in males than in females(2). Clinically, the hallmark symptom of OS is persistent local pain, often intensifying at night, and potentially accompanied by a palpable mass and restricted joint movement(3). A malignant osteoid matrix among tumor cells is pathognomonic, facilitating diagnosis. Despite the use of various treatment modalities, including surgery and neoadjuvant chemotherapy, the outcomes

remain unsatisfactory, with significant adverse effects(4). To develop more effective therapeutic strategies for osteosarcoma, it is essential to uncover the molecular pathways driving its progression. Among them, autophagy, a biological process wherein damaged organelles and proteins are broken down and recycled, is now known to have a significant role in the development of tumors(5). For instance, a study has demonstrated that apatinib can prevent OS growth by causing OS cells to undergo autophagy(6). Another study highlighted that autophagy modulation could increase OS cell sensitivity to chemotherapeutic agents, thereby improving treatment outcomes(7). These findings emphasize the complex function of autophagy in OS and imply that targeting this pathway could offer promising therapeutic strategies for this challenging malignancy.

The intricate regulation of tumor development and treatment response in cancer is governed by several key signaling pathways, with the mTOR and Stat3 pathways being particularly critical in OS(8). The mTOR pathway, a key modulator of metabolism and cell development, frequently acts to promote tumor growth by inhibiting cellular processes that would otherwise suppress malignancy, such as autophagy(9). In OS, mTOR activation has been associated with enhanced tumor cell proliferation and survival, as exemplified by studies showing that *LHX2* promotes OS cell proliferation and metastasis through mTOR pathway activation(10). Conversely, Stat3 is a transcription factor that governs various gene expressions implicated in cell proliferation, survival, and immune responses(11). Stat3 plays a large part in OS progression, and studies have shown that its activation can inhibit processes that would otherwise limit tumor growth, such as autophagy, thereby increasing OS cell survival and resistance to chemotherapy(12). Moreover, the interplay between the mTOR and Stat3 pathways has been identified as a critical axis in OS, where simultaneous targeting of these pathways could induce tumor cell death through the reactivation of suppressed cellular processes(13). These insights suggest that therapeutic strategies aimed at modulating the mTOR/Stat3 signaling axis hold promise for the treatment of this aggressive malignancy.

Ferroptosis, an iron-dependent form of regulated cell death driven by lipid peroxidation, is tightly regulated by cellular redox homeostasis and autophagy. Due to its unique mechanism of cell death compared to other types of cells, it has attracted widespread attention in cancer research(14). Key features of ferroptosis include damage to the cell membrane, mitochondrial shrinkage, and inactivation of glutathione peroxidase 4 (GPX4), causing oxidative damage and the build-up of fatal reactive oxygen species (ROS)(15). Recent studies highlight that autophagy contributes to ferroptosis through selective degradation of iron storage proteins (e.g., ferritin) and lipid droplets, thereby increasing intracellular free iron and peroxidized lipids(16). In the context of OS, ferroptosis is emerging as a possible target for therapy. For example, Bavachin has been shown to increase Fe^{2+} levels and ROS accumulation, reduce glutathione, and induce ferroptosis in OS cells(17). Apolipoprotein E (*APOE*) is primarily known for its role in lipid metabolism. It is currently widely studied in neurodegenerative and cardiovascular diseases such as Alzheimer's disease and atherosclerosis(18-20). Recently, it has been linked to ferroptosis, revealing its broader significance in cancer biology(21). Previous studies have indicated that the overexpression of *APOE* in gastric cancer is connected to increased malignant invasiveness enhanced invasion and lymph node metastasis(22). Additionally, *APOE* appears to regulate intracellular antioxidant defenses, suggesting its potential role in modulating sensitivity to ferroptosis(23). Nevertheless, the function of *APOE* in OS is still mostly unexplored. Given the limited research on *APOE* in OS, this study seeks to investigate *APOE* as a central gene in OS, particularly with ferroptosis, to uncover its potential as a therapeutic target.

This investigation aims to assess the function of *APOE* in the progression of OS, with a particular emphasis on its regulatory impact on ferroptosis, autophagy, and iron metabolism. In particular, the effects of *APOE* overexpression on key cellular processes, including migration, proliferation, invasion, and epithelial-mesenchymal transition (EMT), were investigated in OS cells. Furthermore, the interactions between *APOE* and the mTOR/Stat3 signaling pathway were investigated and evaluated for their effects on

autophagy and ferroptosis in OS. Using *in vitro* cell models and *in vivo* mouse xenografts, this research aims to elucidate the molecular processes by which *APOE* regulates OS progression and evaluate its capacity as a target for therapy.

Material and methods

Weighted gene co-expression network analysis (WGCNA) for identification of the key gene module in OS

The GSE28424 dataset, obtained from the Gene Expression Omnibus (GEO; https://www.ncbi.nlm.nih.gov/geo/query/acc.cgi?acc=GSE28424), was utilized in this study, which includes 19 osteosarcoma (OS) samples and 4 normal bone samples as controls. All genes in the GSE28424 dataset were comprehensively analyzed using the WGCNA method. The gene co-expression network was created by the Bioinfo Intelligent Cloud website (https://www.bic.ac.cn/BIC/#/). To ensure a scale-free topological structure, the optimal soft threshold power was precisely adjusted to $\beta = 16$. After the network was constructed, the weighted adjacency matrix was converted into a topological overlap matrix (TOM) as a robust measure of network connectivity. Hierarchical clustering of the TOM was performed to obtain a dendrogram. In this structure, each branch (represented by different colors) represents a different gene module. The weighted correlation coefficient was used to merge gene fragments with similar expression paths into the relevant modules. Finally, we assessed the correlation between these gene modules and the clinical characteristics of OS to identify the primary section modules potentially associated with OS progression and prognosis.

Screening of differentially expressed genes (DEGs) and performing intersection analysis

DEGs were identified from the GSE28424 dataset utilizing the limma package in R (version 4.0). Gene expression fold changes (FC) greater than 2 were classified as up-regulated genes, while those with FC less than 0.5 were considered down-regulated genes. The criterion for statistical significance was established at $p < 0.05$. The R ggplot2 package (https://cran.r-project.org/package=ggplot2) was employed to

visualize the DEGs. Subsequently, the Bioinformatics and Evolutionary Genomics website (http://bioinformatics.psb.ugent.be/webtools/Venn/) was used to conduct an intersection analysis between the key module genes identified from the WGCNA and all DEGs from the GSE28424 dataset, allowing for the identification of intersecting genes.

Protein-protein interaction (PPI) network construction and hub gene identification

The PPI network analysis of the intersection genes was performed by the Search Tool for the Retrieval of Interacting Genes (STRING: https://string-db.org/) website. The Cytohubba plugin (version 3.8.2) in Cytoscape was used to identify three key network modules using the Maximum Neighborhood Component (MNC), Maximum Clique Centrality (MCC), and Degree algorithms, and the top ten genes of the three algorithms were analyzed. Then, the genes in the three network modules were again subjected to intersection analysis using the Bioinformatics and Evolutionary Genomics website to obtain the key intersection genes. Then, the expression of these important crossover genes in normal and tumors was analyzed in the SangerBox database (http://sangerbox.com/), and the outcomes showed statistical significance when $p<0.05$.

Cell culture

Cyagen Biosciences (Guangzhou, China) provided the human OS cell lines 143B, MG-63, SW1353, U2OS, SaOS-2, and the equivalent normal osteoblastic cell line HOB. The aforementioned cell lines were grown at 37˚C in a humidified incubator with 5% CO_2 in Dulbecco's modified Eagle's medium (DMEM; Sangon, Shanghai, China), supplemented with 10% fetal bovine serum (FBS; Sangon, Shanghai, China) and 100U/mL penicillin/streptomycin solution (Sangon, Shanghai, China).

Cell transfection

At a density of 5×10^5 cells per well, cells were seeded onto 6-well plates and cultured for 24 hours. Upon reaching 70-80% confluence, cells were transfected with APOE

overexpression vectors applying Lipofectamine™ 2000 (10 μL per well; Invitrogen, Shanghai, China) by the manufacturer's protocol. The negative control was an empty vector. The transfection mixtures were incubated for 20 minutes at room temperature and then incorporated into the culture dishes containing 143B and U2OS cells in serum-free medium. After 48 hours of incubation, transfected cells received treatment with 10 μM 3-methyladenine (3-MA; Topscience, Shanghai, China), an autophagy inhibitor, for 24 hours at 37°C. Cells were subsequently harvested for further experiments.

Quantitative real-time reverse transcription PCR (qRT-PCR)

Trizol reagent (Tiangen, Beijing, China) was applied to extract total RNA from cells and tissues under the manufacturer's instructions. Agilent 2100 Bioanalyzer (Agilent, Shanghai, China) served to evaluate the quality of the RNA. Complementary DNA (cDNA) was synthesized from the isolated RNA using the PrimeScripTM RT reagent kit (Takara, Shanghai, China) according to the manufacturer's instructions. Quantitative RT-PCR was conducted using Bio-Rad instruments (Bio-Rad, Shanghai, China) with SYBR Green reagent (TaKaRa, Dalian, China) in duplicate reactions. All qRT‐PCR results were analyzed using $2^{-\Delta\Delta Ct}$ values and normalized to glyceraldehyde-3-phosphate dehydrogenase (GAPDH), which served as the internal control. Primer sequences for amplification are shown in Tables 1 and 2.

Western blot (WB) assay

Total protein was extracted from cells and tissues utilizing RIPA buffer (Beyotime, Shanghai, China). The Protein Concentration Kits (Beyotime, Shanghai, China) were applied to calculate the protein concentration. Following a 5-minute boil at 98°C, the samples' total proteins were separated using 10% sodium dodecyl sulfate-polyacrylamide gel electrophoresis (SDS-PAGE) and moved to membranes made of PVDF (Beyotime, Shanghai, China). The primary antibodies were then incubated on the membranes for a whole night at 4°C after they had been blocked for one hour at room temperature with 5% nonfat milk. The next day, secondary antibodies (Sanying, Wuhan, China) coupled with horseradish peroxidase (HRP) were incubated on the

membranes for one hour at room temperature. Protein bands were detected utilizing enhanced chemiluminescence (ECL) reagents (Beyotime, Shanghai, China) and visualized with the Image J software. The following primary antibodies were employed in this investigation: APOE (1:1000), N-cadherin (1:2000), E-cadherin (1:20000), Vimentin (1:2000), p-mTOR (1:2000), mTOR (1:5000), p-Stat3 (1:1000), Stat3 (1:2000), Beclin1 (1:1000), LC3B-1 (1:1000), LC3B-2 (1:1000), p62 (1:5000), TfR1 (1:1000), FPN (1:2000), GPX4 (1:1000), SLC7A11 (1:1000), and GAPDH (1:5000). All antibodies were sourced from Sanying (Wuhan, China).

Cell Counting Kit-8 (CCK-8) assay

Cell proliferation was measured via the CCK-8 kit (Yeasen, Shanghai, China). After being equally plated at a density of 1×10^3 cells per well in a 96-well plate, the cells were grown for 1, 2, 3, 4, and 5 days. After that, 10 μL of CCK-8 reagent was added to each well. The optical density (OD) of each well at 450 nm was measured by a microplate reader (Bio-Rad, Shanghai, China) to investigate the viability of the cells.

Transwell assay

Transwell assays were conducted to assess the capacity of OS 143B and U2OS cells to invade and migrate. For the invasion assay, the upper chambers of Transwell plates (Corning, Shanghai, China) were pre-coated with 40 μL of Matrigel (BD Biosciences, Shanghai, China) and solidified for 30 min at 37°C. Each Transwell chamber had an upper chamber holding around 5×10^4 cells suspended in 200 μl of DMEM media without FBS, and a bottom chamber holding 600 μl of DMEM containing 10% FBS. After incubation for 24 h at 37 °C, cells were dyed with DAPI (Beyotime, Shanghai, China) at for 15 min 37 °C and counted under an optical microscope (Nikon, Shanghai, China). For the migration assay, cells were seeded into Matrigel-uncoated upper chambers. The residual procedures were identical to those used in the invasion tests.

Flow cytometry

For apoptosis analyses, the cells were recognized by flow cytometry utilizing the

Annexin V-PE/FITC apoptosis detection kit (Beyotime, Shanghai, China). The transfected 143B and U2OS cells were detached using trypsin-EDTA (Absin, Shanghai, China). The cells were cleaned with phosphate-buffered saline (PBS) following treatment. After that, the cells were again suspended in 1× binding buffer that the Annexin V-FITC apoptosis detection kit had supplied. Each 100 μL cell suspension in binding buffer received 5 μL of Propidium Iodide (PI) and 5 μL of Annexin V-FITC. After giving the cells a gentle vortex, they were incubated for 30 minutes in the dark at room temperature. After staining, each sample received 400 μL of 1× binding buffer, for a total volume of 500 μL. A BD FACSCalibur flow cytometer (BD Biosciences, NJ, USA) was applied to collect the data. For every sample, at least 10,000 occurrences were recorded. With the use of FlowJo software (FlowJo LLC, Oregon, USA), flow cytometry data were examined.

Detection of ROS level

With a ROS test kit (Jiancheng, Nanjing, China), intracellular ROS levels were measured. 143B and U2OS cells that had been transfected were treated for 30 minutes at 37 °C in the dark with the DCFH-DA fluorescent probe (Beyotime, Shanghai, China). To get rid of extra dye, the cells were thrice rinsed with PBS after incubation. An excitation wavelength of 488 nm and an emission wavelength of 525 nm was employed to measure the fluorescence intensity, which is a good indicator of ROS levels, using a microplate reader (Bio-Rad, Shanghai, China).

Detection of superoxide dismutase (SOD)

The SOD level was determined via a SOD assay kit (Beyotime, Shanghai, China). The lysis buffer included in the kit was used to lyse OS cells. To extract supernatant and eliminate cell debris, cell lysates were centrifuged at 10,000 x g for 4°C. An assay kit for BCA protein (Beyotime, Shanghai, China) was employed to measure the protein content. With SOD assay buffer, protein samples were diluted. In accordance with the manufacturer's proposals, SOD levels were assessed by a SOD test kit. By utilizing a microplate reader (Bio-Rad, Shanghai, China), absorbance was determined at 450 nm.

Measurement of glutathione (GSH)

A GSH assay kit (Jiancheng, Nanjing, China) was performed to quantify the GSH levels. The transfected 143B and U2OS cells were washed with cold PBS, and lysed in a GSH assay buffer provided by the GSH assay kit. After removing any debris from the cell lysates with a 10-minute, 10,000-x-g centrifugation at 4°C, the supernatants were separated and saved for further examination. The GSH levels were detected by following the manufacturer's protocol, which involves a two-step enzymatic reaction that converts GSH into a measurable form. A microplate reader (Bio-Rad, Shanghai, China) was utilized to quantify the absorbance at 405 nm.

Measurement of malondialdehyde (MDA)

The test kit for lipid peroxidation MDA (Jiancheng, Nanjing, China) was carried out to assess the MDA levels. Transfected 143B and U2OS cells were rinsed with ice-cold PBS, lysed using RIPA lysis buffer (Beyotime, Shanghai, China), and subjected to centrifugation at 10,000 x g for 10 minutes at 4 °C. To measure the amount of MDA and the concentration of protein, the supernatant was collected. The sample was then heated for 15 minutes in a mixture of 0.1 mL and 0.2 mL MDA solution. Utilizing a microplate reader (Bio-Rad, Shanghai, China), the absorbance at 532 nm was determined once the sample had cooled to room temperature.

Iron assay

The levels of Fe^{2+} and total iron were measured via an iron assay kit (Abcam, Shanghai, China). Cells were homogenized on ice in an iron assay buffer, and the supernatants were collected. To measure Fe^{2+} and total iron levels, samples were treated with iron buffer and an iron-reducing agent. The iron probe was added to each sample, and the mixtures were cultivated for 60 minutes at room temperature. The microplate reader (Bio-Rad, Shanghai, China) was utilized to measure the absorbance at 593 nm.

Mouse xenograft experiments

All animal experiments were conducted strictly in compliance with the policies and procedures authorized by the Ethics Committee of Zhongshan Hospital Minhang Branch, Fudan University (approval number: 2024-MHYY-534). Shulaibao Biotech (Wuhan, China) supplied male nude mice that were 4-5 weeks old. They were kept in standard laboratory conditions with unrestricted access to water and food. Two groups were arbitrarily selected for the mice (n=6 per group): the Vector group, injected subcutaneously with 5×10^6 143B cells carrying a control vector, and the over-*APOE* group, injected with 5×10^6 143B cells overexpressing *APOE*. Injections were given on the right side of every mouse. Every week, the size and length of the tumors were measured utilizing calipers to track their growth. Tumor volume was computed with the following formula: Volume = (length × width²)/2. The mice were put to death with 2% pentobarbital sodium (150 mg/kg) administered intraperitoneally after four weeks, following ethical guidelines. Tumors were excised, weighed, and captured on camera. After being removed, the tumors were quickly frozen in liquid nitrogen and kept for further examination at -80°C. All procedures were conducted in compliance with the principles of the 3Rs (Replacement, Reduction, and Refinement) to ensure ethical experimentation.

Statistical analysis

The R programming language is utilized for statistical evaluation. Every experiment was conducted three separate times on its own. The Data are expressed as mean ± SD. The Student's t-test with two tails was employed to compare the two groups. For comparisons among several groupings, one-way analysis of variance (ANOVA) followed by Tukey's post-hoc test was employed. At $p < 0.05$, statistical significance was established.

Results

Identification of gene co-expression networks and modules

For a scale-free topological model fit, 16 was shown to be the ideal soft threshold power (Figure 1A). The dendrogram of the GSE28424 samples showed no outliers (Figure

1B). Based on their patterns of co-expression across samples, genes were categorized into several modules, and every module was assigned a different color (Figure 1C). To unravel the connections among these identified modules, the characteristic gene adjacencies were carefully examined (Figure 1D). Among the different modules, the purple module and the samples have a correlation value of 0.817, indicating a significant relationship (Figure 1E). This significant correlation emphasizes the potential biological relevance of the genes within the cyan module to the GSE28424 dataset.

Identification of key genes in OS through PPI network analysis and determination of the hub gene

Differential expression analysis was performed on the GSE28424 dataset, resulting in the identification of 498 up-regulated and 869 down-regulated genes (Figure 2A). T From the purple module and DEGs in GSE28424, 56 intersection genes were identified (Figure 2B). These intersection genes were analyzed by PPI network construction, and the top 10 genes based on MCC, MNC, and Degree algorithms were visualized using Cytoscape. In the MCC, MNC, and Degree networks, there are ten nodes and twenty edges each (Figures 2C, 2D, and 2E). After that, the top 10 genes of the three algorithms were analyzed again, and nine key intersection genes were obtained (Figure 2F). The expression levels of these nine genes (*APOE*, *CEBPA*, *DCN*, *FOXO1*, *GPX3*, *HMOX1*, *KLF2*, *MGP,* and *SPP1*) were examined in the GSE28424 dataset, and it was found that all gene tumor case groups showed lower expression levels (Figure 2G). Given the crucial role of *APOE* in lipid metabolism and its relatively limited exploration in the context of OS, *APOE* was chosen as the focus of this study.

Overexpression of *APOE* inhibits proliferation, migration, and invasion of OS cells

APOE mRNA and protein expression levels were evaluated across various osteosarcoma cell lines (143B, MG-63, SW1353, U2OS SaOS-2,) and compared to normal osteoblastic cells (HOB). In comparison to HOB cells, OS cell lines have greatly reduced APOE mRNA and protein levels, as shown in Figures 3A, 3B, and 3C. After

transfecting U2OS and 143B cells with an APOE overexpression vector, a notable increase in APOE expression was detected at the levels of both mRNA and protein (Figures 3D, 3E, and 3F). Afterward, CCK-8 was employed to recognize the proliferation of OS cells after *APOE* overexpression. The findings demonstrated that in contrast to the control group, *APOE* overexpression significantly inhibited OS cell proliferation (Figures 3G, 3H). Transwell assay was utilized to identify the effect of *APOE* on OS cell invasion and migration. By drastically reducing the quantity of OS cells stained with DAPI in comparison to the control group, APOE overexpression was found to considerably impede the ability of OS cells to invade and migrate (Figures 3I, 3J).

APOE overexpression inhibits OS cell invasion and migration, with effects reversed by autophagy inhibition

Transfected 143B and U2OS cells were subjected to a 24-hour autophagy inhibitor (3-MA) treatment and then subjected to a Transwell assay. The findings demonstrated that in contrast to the Vector Group, *APOE* overexpression inhibited the invasion and migration of OS cells, while 3-MA treatment enhanced the migration and invasion of OS cells. *APOE* overexpression combined with 3-MA treatment can weaken the inhibitory impact of overexpression of *APOE* on the metastatic ability of OS cells (Figure 4A, 4B). Next, qRT-PCR was employed to detect EMT-related markers (*N-cadherin*, *E-cadherin*, and *Vimentin*) expression in OS cells after overexpression of *APOE* and combined with 3-MA treatment (Figures 4C, 4D). As contrasted to the Vector group, the results indicated that the levels of *Vimentin* and *N-cadherin* in cells overexpressing *APOE* were significantly reduced, as well as the level of *E-cadherin* was markedly elevated. The reverse was observed when EMT-related markers were detected in cells treated with 3-MA. The metastatic potential of OS cells overexpressing APOE to spread might be considerably inhibited by 3-MA treatment. Consistent results were also detected at the protein level (Figures 4E, 4F, 4G, and 4H). These outcomes suggest that *APOE* overexpression inhibits OS cell invasion and migration by regulating EMT, and this effect can be reversed by inhibiting autophagy.

Overexpression of *APOE* stimulates autophagy via the mTOR/Stat3 signaling pathway in OS cells

To investigate the impact of *APOE* overexpression on autophagy in osteosarcoma cells, we examined the expression of key proteins engaged in the mTOR and Stat3 signaling pathways, as well as several autophagy-related markers. WB analysis showed that overexpression of APOE significantly decreased the levels of p-mTOR in both 143B and U2OS cells, while total mTOR levels remained unchanged (Figures 5A, 5B, 4C). Similarly, p-Stat3 levels were reduced in APOE-overexpressing cells without affecting total Stat3 expression (Figures 5D, 5E, 5F). These results indicate that APOE overexpression inhibits the mTOR and Stat3 pathways, both of which are known to negatively regulate autophagy. Further analysis of autophagy markers revealed that *APOE* overexpression resulted in a notable increase in LC3B-1, LC3B-2, and Beclin1 mRNA and protein levels, while levels of p62, a marker of autophagy flux, were decreased in both 143B and U2OS cells (Figures 5G, 5H, 5I, 5J, and 5K). These results indicate an enhanced autophagic activity in *APOE*-overexpressing cells.

***APOE* overexpression induces apoptosis and disrupts iron homeostasis in OS cells**

To determine the impacts of *APOE* overexpression on apoptosis in osteosarcoma cells, flow cytometry was done after Annexin V/PI double staining. The findings demonstrated that, in comparison to the vector control group, the proportion of apoptotic cells increased significantly in both 143B and U2OS cells overexpressing APOE (Figures 6A, 6B). These findings suggest that *APOE* overexpression promotes apoptosis in osteosarcoma cells. Additionally, we evaluated the impact of *APOE* overexpression on oxidative stress markers. *APOE* overexpression led to a significant increase in ROS levels (Figure 6C), and a concurrent increase in intracellular Fe^{2+} levels (Figure 6D), both of which are indicators of enhanced oxidative stress. Conversely, the activities of key antioxidant enzymes were significantly decreased in *APOE*-overexpressing cells compared to controls (Figures 6E, 6G). Furthermore, MDA levels, a marker of lipid peroxidation, were significantly elevated in the *APOE*-overexpressing

cells (Figure 6F). These findings suggest that *APOE* overexpression not only induces apoptosis in osteosarcoma cells but also disrupts iron homeostasis, contributing to increased oxidative stress and compromised antioxidant defenses, which may further potentiate cell death mechanisms.

Overexpression of *APOE* alters iron metabolism in OS cells

Given the tight relationship between iron metabolism and the onset, progression, and metastasis of malignancies, iron metabolism regulatory targets were detected in U2OS and 143B cells. First, the total iron content in U2OS and 143B cells after overexpression of *APOE* was determined using a total iron ion kit. When contrasting with the Vector Group, the total iron content was greatly elevated after overexpression of *APOE* (Figure 7A). Subsequently, qRT-PCR was utilized to determine the levels of *TfR1*, *FPN*, *GPX4*, and *SLC7A11* expression in OS cells after overexpression of *APOE*. In contrast to the control cohort, the level of *TfR1* was markedly increased after overexpression of *APOE*, while the levels of other factors were substantially reduced (Figures 7B, 7C). This was further confirmed at the protein level (Figures 7D, 7E, and 7F). These results indicate that overexpression of *APOE* disrupts iron homeostasis and may promote ferroptosis by changing the expression of iron-regulating markers in OS cells.

***APOE* overexpression reduces tumor growth and modulates ferroptosis-related markers**

A mouse xenograft model was established using 143B cells to assess the impact of *APOE* overexpression *in vivo* tumor growth. Mice injected with *APOE*-overexpressing 143B cells had greatly reduced tumors in comparison to mice given vector control cell injections (Figure 8A, 8B). Further analysis of tumor tissues revealed notable alterations in the expression of key genes involved in ferroptosis and autophagy. Specifically, mRNA levels of *LC3B-1*, *LC3B-2*, and *TfR1* were upregulated in tumors from the *APOE*-overexpressing group, while *GPX4*, *SLC7A11*, and *FPN* were downregulated (Figure 8C). These changes were confirmed at the protein level, with LC3B-1, LC3B-2, and TfR1 consistently upregulated, and GPX4, SLC7A11, and FPN

downregulated (Figure 8D, 8E). These findings suggest that *APOE* overexpression not only inhibits tumor growth *in vivo* but also promotes autophagy and disrupts iron homeostasis, potentially enhancing ferroptosis of osteosarcoma cells in the tumor microenvironment. Supplementary Figure 1 summarizes the molecular mechanisms through which *APOE* overexpression influenced osteosarcoma progression. The figure illustrates how *APOE* activated the mTOR/Stat3 signaling pathway, thereby promoting autophagy while disrupting iron homeostasis and inducing ferroptosis. Collectively, these processes inhibited cell proliferation, invasion, migration, and tumor growth, as observed in both *in vivo* and *in vitro* models.

Discussion

OS is a particularly aggressive bone malignancy that predominantly affects adolescents and children(24). Genetic studies have identified several key genes implicated in OS pathogenesis. For instance, mutations in *TP53* are frequently observed in OS and are linked to genomic instability(25). *MYC* overexpression is associated with poor prognosis, while *SPP1* levels are significantly elevated in OS(26, 27). Additionally, *KLF2* has been shown to prevent the growth and invasion of OS cells, and the curcumin analogue EF24 upregulates *HMOX1* expression, promoting ferroptosis in OS cells(28, 29). APOE is primarily known for its role in lipid metabolism and has been widely studied in various cancers. In ovarian cancer, *APOE* is linked to the survival and development of cancer cells; in gastric cancer, its overexpression is linked to increased invasiveness; in breast cancer, it affects tumor cell proliferation and migration; and in prostate cancer, it is involved in apoptosis resistance(30-32). However, the role of *APOE* in OS remains understudied. Given its critical role in other malignancies, understanding the function of *APOE* in OS could offer novel viewpoints on the pathogenesis of this disease. This research used bioinformatics analysis to reveal that *APOE* is significantly downregulated in OS. Functional experiments showed that *APOE* overexpression inhibited OS cell growth while promoting cell apoptosis. These findings implied that *APOE* may be essential to the development of OS and serve as a potential therapeutic target for this aggressive tumor.

Autophagy, a critical lysosomal degradation process essential for cellular homeostasis, maintains homeostasis by recycling damaged or unnecessary cellular components(33). It exhibits a dual role in overall survival (OS) by either inhibiting tumor progression or enabling cancer cells to survive under stressful conditions. Our study demonstrates that *APOE* overexpression exerts potent anti-tumor effects in OS by suppressing the mTOR/Stat3 signaling axis, a central regulator of cellular metabolism and survival. Mechanistically, *APOE* overexpression significantly reduced phosphorylation of mTOR and Stat3, thereby alleviating their repression of autophagy and triggering enhanced autophagic flux, as evidenced by elevated LC3B-II/LC3B-I ratios, upregulated Beclin1, and diminished p62 accumulation. Key autophagy markers also play crucial roles in tumor dynamics. For instance, luteolin has been shown to increase Beclin1 expression in OS cells to promote autophagy and augment doxorubicin-induced autophagy(34). Additionally, p62 overexpression is linked to aggressive characteristics and a poor prognosis in OS, as its accumulation inhibits autophagy(35). Concurrently, mTOR/Stat3 inhibition disrupted iron homeostasis, downregulating ferroptosis suppressors (GPX4, SLC7A11) while upregulating TfR1, which collectively drove iron overload, lipid peroxidation, and ferroptotic cell death. This dual mechanism—autophagy activation coupled with ferroptosis induction—highlights APOE's unique role in rewiring OS cell fate. In cancer cells, autophagy plays a complex and multifaceted role, making it a challenging but promising therapeutic target. In OS, autophagy has been implicated in various aspects of tumor biology. For example, autophagy can reduce the effectiveness of chemotherapeutic agents such as cisplatin, doxorubicin, and methotrexate in OS cells(36). Conversely, miR-101 has been shown to downregulate autophagy, thereby inhibiting OS cell proliferation and metastasis(37). These findings suggest that targeting autophagy could be an effective strategy to overcome chemotherapy resistance and reduce metastasis in OS.

The regulation of autophagy is intricately linked to several signaling pathways, with mTOR and Stat3 being central regulators. Our study demonstrated that *APOE*

overexpression in OS cells not only altered iron metabolism and induced ferroptosis but also activated the mTOR/Stat3 signaling pathway. mTOR acts as a crucial autophagy-negative regulator, and its inhibition is associated with the induction of autophagy and subsequent cancer cell death. For instance, rapamycin inhibits tumor growth by promoting autophagy through mTOR pathway inhibition(38). Stat3, a downstream effector of mTOR, mediates the expression level of multiple genes implicated in the development of cancer. In OS, *BLACAT1* upregulation has been shown to regulate Stat3 phosphorylation, thereby enhancing OS progression(39). Our findings reveal that APOE overexpression promotes autophagy in OS cells by the mTOR/Stat3 pathway, underscoring the potential therapeutic benefit of targeting APOE alongside autophagy inhibition in OS treatment. *In vivo*, *APOE* overexpression significantly slowed tumor growth, with molecular analyses suggesting that mTOR/Stat3 activation by *APOE* contributes to OS suppression by enhancing autophagy and ferroptosis. The mTOR/Stat3 signaling pathway is also closely associated with ferroptosis. Abnormal activation of this pathway has been linked to tumorigenesis and resistance to therapy in various cancers. For example, *CD151* knockdown in OS reduces mTOR phosphorylation, inhibiting tumor progression, while natural compounds like alternol suppress OS cell proliferation by modulating Stat3, causing cell cycle arrest and apoptosis(40, 41). Additionally, Stat3 is involved in oxidative responses, influencing ferroptosis regulation. Inhibiting Stat3 has been shown to block ferroptosis in pancreatic ductal adenocarcinoma and induce it in breast cancer(42). These findings suggest that targeting the mTOR/Stat3 signaling pathway in combination with *APOE* modulation could offer a novel therapeutic strategy for managing OS.

Ferroptosis, a kind of non-apoptotic cell death that is dependent on iron, is described by iron overload and lipid hydroperoxide accumulation, making it closely regulated by iron metabolism(43). Iron metabolism and ferroptosis have been shown to be important components of cancer biology in growing body of research. For instance, FANCD2 silencing has been shown to inhibit OS growth by regulating the JAK2/Stat3 axis and inducing ferroptosis(44). PEITC induces ferroptosis in OS cells through activation of

the ROS-related MAPK signaling pathway, and baicalin inhibits the development of OS cells both in vitro and in vivo by promoting ferroptosis(45, 46). Building on these discoveries, our research investigated the function of APOE in ferroptosis regulation in OS cells. We demonstrated that APOE overexpression significantly altered iron metabolism, leading to increased levels of ROS and Fe^{2+}, along with decreased SOD and GSH activities, which are indicative of oxidative stress and lipid peroxidation. These changes resulted in the downregulation of key ferroptosis regulatory genes such as GPX4 and SLC7A11, while TfR1 was upregulated, collectively driving ferroptosis in OS cells. In vivo experiments further confirmed that APOE overexpression led to reduced tumor growth, with molecular analyses revealing corresponding changes in autophagy and ferroptosis markers. These results highlight the therapeutic potential of targeting APOE and iron metabolism pathways in treating osteosarcoma. This contrasts with studies in other contexts, such as neurodegenerative diseases, where *APOE* is reported to inhibit ferroptosis(47). The opposing effects likely stem from tissue-specific lipid metabolism, signaling pathway crosstalk, and experimental model variations. In OS, overexpression of *APOE* inhibits the mTOR/Stat3 pathway, making cells sensitive to ferroptosis, while in other contexts, the anti-ferroptotic effect of *APOE* may involve activation of the PI3K/AKT pathway to inhibit ferritin phagocytosis(47). Finally, our study employed exogenous *APOE* overexpression, which may disrupt physiological lipid trafficking and create an artificial pro-oxidant state, contrasting with studies of endogenous *APOE* in neurons or hepatocytes that reflect its role in maintaining lipid homeostasis under basal conditions.

While our findings demonstrate that *APOE* overexpression suppresses osteosarcoma progression by modulating autophagy and ferroptosis, it is important to contextualize these results within the broader biological roles of APOE. Notably, *APOE* is a multifunctional protein with well-documented roles in lipid metabolism. Previous studies have shown that *APOE* overexpression in hepatic or systemic contexts can induce hypertriglyceridemia (HTG) by impairing triglyceride clearance, which is linked to metabolic disorders and an elevated risk of certain cancers(48-51). For instance,

elevated serum triglycerides (TGs) may promote tumorigenesis through chronic inflammation, oxidative stress, or lipid peroxidation-driven genomic instability(52). However, the role of *APOE* in cancer appears to be highly context-dependent, varying by tissue type, tumor microenvironment, and molecular pathways involved. In contrast to its pro-tumorigenic effects in some cancers, our data reveal that *APOE* overexpression in osteosarcoma cells significantly inhibits proliferation, migration, and invasion while inducing ferroptosis. This discrepancy may arise from tissue-specific signaling mechanisms. In this study, it was found that overexpression of *APOE* inhibits the mTOR/Stat3 pathway in OS, which has been shown in previous studies to be a key driver of tumor progression and treatment resistance (8). Conversely, *APOE* produces immunosuppression through CXCL1 mediated by NF-κB in pancreatic cancer and promotes tumor growth (53). Furthermore, the relationship between hypertriglyceridemia and cancer risk is complex and not universally applicable. While epidemiological studies associate HTG with increased cancer incidence, this correlation may not extend to all cancer types or stages. Osteosarcoma, a malignancy with distinct genetic and metabolic profiles, may respond differently to lipid metabolic perturbations. Our findings suggest that *APOE*'s anti-tumor effects in OS are mediated through autophagy activation and iron homeostasis disruption, rather than systemic lipid alterations. Importantly, our xenograft model focused on localized tumor suppression without inducing systemic hypertriglyceridemia, highlighting the potential for tissue-targeted *APOE* modulation as a therapeutic strategy.

There are three isomers of *APOE*: *ApoE2*, *ApoE3*, and *ApoE4*, and our main focus is on *ApoE4*. Our study reveals that *APOE4* overexpression promotes autophagy in osteosarcoma cells, contrasting with its autophagy-suppressive effects in neurodegenerative contexts(54, 55). This divergence likely stems from tissue-specific signaling networks and metabolic demands. In OS, *APOE*4-driven lipid remodeling may inhibit mTOR/Stat3 signaling, a key suppressor of autophagy, thereby activating pro-degradative pathways. Conversely, in neurons, *APOE4* disrupts lysosomal function and autophagosome clearance, exacerbating proteotoxic stress. These findings

underscore the context-dependent duality of *APOE* isoforms and highlight the need to explore their roles across disease models.

Future studies should investigate whether *APOE* overexpression in OS influences systemic lipid metabolism or interacts with dietary/endocrine factors to modulate tumor progression. Additionally, exploring tissue-specific isoforms of *APOE* (e.g., *APOE2*, *APOE3*, *APOE4*) and their differential effects on cancer biology could provide further mechanistic insights. These efforts will clarify the dual roles of *APOE* in metabolism and oncology, guiding its safe therapeutic application.

Conclusion

This research elucidates the crucial function of *APOE* in the regulation of OS progression through its effects on autophagy and ferroptosis. The results demonstrated that *APOE* overexpression in OS cells markedly suppressed cell proliferation, invasion, and migration while causing ferroptosis and apoptosis. From a mechanistic perspective, *APOE* activated the mTOR/Stat3 signaling pathway, thereby enhancing autophagic activity. Concurrently, *APOE* disrupted iron homeostasis, which resulted in increased ROS levels, lipid peroxidation, and ferroptosis. These findings were corroborated by in vivo experiments, wherein *APOE* overexpression resulted in significantly reduced tumor growth and altered expression of key autophagy and ferroptosis markers. Our results suggest that targeting *APOE*, in conjunction with the modulation of iron metabolism and the mTOR/Stat3 signaling pathway, could offer a novel therapeutic approach for managing osteosarcoma. Future studies should explore the potential of combining *APOE* modulation with existing therapies to enhance treatment efficacy in OS.

Authors' Contribution

Conception and design of the research: Xiangyang Cheng and Liang Wu

Acquisition of data: Xiangyang Cheng

Analysis and interpretation of data: Xiangyang Cheng, Yiming Zhang, Chong Bian, Huijie Gu, and Guangnan Chen

Statistical analysis: Yiming Zhang, Chong Bian, Huijie Gu, and Guangnan Chen

Drafting the manuscript: Xiangyang Cheng

Revision of manuscript for important intellectual content: Liang Wu

Ethics approval and consent to participate

Not applicable.

Consent for publication

Not applicable.

Availability of data and materials

The datasets used and/or analyzed during the current study are available from the corresponding author upon reasonable request.

Competing interests

The authors have no conflicts of interest to declare.

Funding

This study was funded by Shanghai Minhang District Natural Science Foundation, China(2023MHZ087).

Acknowledgments

None.

References

1. Czarnecka AM, Synoradzki K, Firlej W, Bartnik E, Sobczuk P, Fiedorowicz M, et al. Molecular biology of osteosarcoma. Cancers. 2020;12(8):2130.

2. Beird HC, Bielack SS, Flanagan AM, Gill J, Heymann D, Janeway KA, et al. Osteosarcoma. Nature reviews Disease primers. 2022;8(1):77.
3. Zarghooni K, Bratke G, Landgraf P, Simon T, Maintz D, Eysel P. The diagnosis and treatment of osteosarcoma and Ewing's sarcoma in children and adolescents. Deutsches Ärzteblatt International. 2023;120(24):405.
4. Tsukamoto S, Errani C, Angelini A, Mavrogenis AF. Current treatment considerations for osteosarcoma metastatic at presentation. Orthopedics. 2020;43(5):e345-e58.
5. Vitto VAM, Bianchin S, Zolondick AA, Pellielo G, Rimessi A, Chianese D, et al. Molecular mechanisms of autophagy in cancer development, progression, and therapy. Biomedicines. 2022;10(7):1596.
6. Liu K, Ren T, Huang Y, Sun K, Bao X, Wang S, et al. Apatinib promotes autophagy and apoptosis through VEGFR2/STAT3/BCL-2 signaling in osteosarcoma. Cell Death & Disease. 2017;8(8):e3015-e.
7. Pu Y, Wang J, Wang S. Role of autophagy in drug resistance and regulation of osteosarcoma. Molecular and Clinical Oncology. 2022;16(3):1-6.
8. Wang Yt, Tang F, Hu X, Zheng Cx, Gong Tj, Zhou Y, et al. Role of crosstalk between STAT3 and mTOR signaling in driving sensitivity to chemotherapy in osteosarcoma cell lines. IUBMB life. 2020;72(10):2146-53.
9. Marafie SK, Al-Mulla F, Abubaker J. mTOR: Its Critical Role in Metabolic Diseases, Cancer, and the Aging Process. International Journal of Molecular Sciences. 2024;25(11):6141.
10. Song H, Liu J, Wu X, Zhou Y, Chen X, Chen J, et al. LHX2 promotes malignancy and inhibits autophagy via mTOR in osteosarcoma and is negatively regulated by miR-129-5p. Aging (Albany NY). 2019;11(21):9794.
11. Hu Y, Dong Z, Liu K. Unraveling the complexity of STAT3 in cancer: molecular understanding and drug discovery. Journal of Experimental & Clinical Cancer Research. 2024;43(1):23.
12. Liu Y, Liao S, Bennett S, Tang H, Song D, Wood D, et al. STAT3 and its targeting inhibitors in osteosarcoma. Cell proliferation. 2021;54(2):e12974.
13. Ji Z, Shen J, Lan Y, Yi Q, Liu H. Targeting signaling pathways in osteosarcoma: Mechanisms and clinical studies. MedComm. 2023;4(4):e308.
14. Zhou Q, Meng Y, Li D, Yao L, Le J, Liu Y, et al. Ferroptosis in cancer: From molecular mechanisms to therapeutic strategies. Signal Transduction and Targeted Therapy. 2024;9(1):55.
15. Consoli V, Fallica AN, Sorrenti V, Pittala V, Vanella L. Novel insights on ferroptosis modulation as potential strategy for cancer treatment: when nature kills. Antioxidants & Redox Signaling. 2024;40(1):40-85.
16. Chen F, Cai X, Kang R, Liu J, Tang D. Autophagy-Dependent Ferroptosis in Cancer. Antioxidants & redox signaling. 2023;39(1-3):79-101.
17. Luo Y, Gao X, Zou L, Lei M, Feng J, Hu Z. Bavachin induces ferroptosis through the STAT3/P53/SLC7A11 axis in osteosarcoma cells. Oxidative medicine and cellular longevity. 2021;2021(1):1783485.
18. Serrano-Pozo A, Das S, Hyman BT. APOE and Alzheimer's disease: advances in

genetics, pathophysiology, and therapeutic approaches. The Lancet Neurology. 2021;20(1):68-80.
19. Zhao J, Gomes D, Yuan F, Feng J, Zhang X, O'Toole TE. Oral Polystyrene Consumption Potentiates Atherosclerotic Lesion Formation in ApoE(-/-) Mice. Circulation research. 2024;134(9):1228-30.
20. Alagarsamy J, Jaeschke A, Hui DY. Apolipoprotein E in Cardiometabolic and Neurological Health and Diseases. International journal of molecular sciences. 2022;23(17).
21. Wu L, Xian X, Tan Z, Dong F, Xu G, Zhang M, et al. The role of iron metabolism, lipid metabolism, and redox homeostasis in Alzheimer's disease: from the perspective of ferroptosis. Molecular Neurobiology. 2023;60(5):2832-50.
22. Peng X, Cai Z, Chen D, Ye F, Hong L. Prognostic significance and immune characteristics of APOE in gastric cancer. Aging (Albany NY). 2023;15(23):13840.
23. Belaidi AA, Masaldan S, Southon A, Kalinowski P, Acevedo K, Appukuttan AT, et al. Apolipoprotein E potently inhibits ferroptosis by blocking ferritinophagy. Molecular psychiatry. 2024;29(2):211-20.
24. Argenziano M, Tortora C, Pota E, Di Paola A, Di Martino M, Di Leva C, et al. Osteosarcoma in children: not only chemotherapy. Pharmaceuticals. 2021;14(9):923.
25. Synoradzki KJ, Bartnik E, Czarnecka AM, Fiedorowicz M, Firlej W, Brodziak A, et al. TP53 in biology and treatment of osteosarcoma. Cancers. 2021;13(17):4284.
26. De Noon S, Ijaz J, Coorens TH, Amary F, Ye H, Strobl A, et al. MYC amplifications are common events in childhood osteosarcoma. The Journal of Pathology: Clinical Research. 2021;7(5):425-31.
27. Zhang Z, Liu B, Lin Z, Mei L, Chen R, Li Z. SPP1 could be an immunological and prognostic biomarker: From pan‐cancer comprehensive analysis to osteosarcoma validation. The FASEB Journal. 2024;38(14):e23783.
28. Wang H, Han J, Dmitrii G, Ning K, Zhang Xa. KLF transcription factors in bone diseases. Journal of Cellular and Molecular Medicine. 2024;28(8):e18278.
29. Lin H, Chen X, Zhang C, Yang T, Deng Z, Song Y, et al. EF24 induces ferroptosis in osteosarcoma cells through HMOX1. Biomedicine & Pharmacotherapy. 2021;136:111202.
30. Wu C, Li T, Cheng W. The correlation between APOE expression and the clinical characteristics and prognosis of patients with endometrial cancer. Medicine. 2022;101(37):e30536.
31. Gan C, Zhang Y, Liang F, Guo X, Zhong Z. Effects of APOE gene ε4 allele on serum lipid profiles and risk of cardiovascular disease and tumorigenesis in southern Chinese population. World Journal of Surgical Oncology. 2022;20(1):280.
32. Zhou Y, Luo G. Apolipoproteins, as the carrier proteins for lipids, are involved in the development of breast cancer. Clinical and Translational Oncology. 2020;22(11):1952-62.
33. Liu S, Yao S, Yang H, Liu S, Wang Y. Autophagy: Regulator of cell death. Cell death & disease. 2023;14(10):648.
34. Ashrafizadeh M, Ahmadi Z, Farkhondeh T, Samarghandian S. Autophagy regulation using luteolin: new insight into its anti-tumor activity. Cancer Cell International. 2020;20(1):537.

35. Lu Y, Wang Q, Zhou Y, Sun L, Hu B, Xue H, et al. Overexpression of p62 is associated with poor prognosis and aggressive phenotypes in osteosarcoma. Oncology Letters. 2018;15(6):9889-95.
36. Liao Y-X, Lv J-Y, Zhou Z-F, Xu T-Y, Yang D, Gao Q-M, et al. CXCR4 blockade sensitizes osteosarcoma to doxorubicin by inducing autophagic cell death via PI3K-Akt-mTOR pathway inhibition. International Journal of Oncology. 2021;59(1):1-11.
37. Chang Z, Huo L, Li K, Wu Y, Hu Z. Blocked autophagy by miR‐101 enhances osteosarcoma cell chemosensitivity in vitro. The Scientific World Journal. 2014;2014(1):794756.
38. Zou Z, Tao T, Li H, Zhu X. mTOR signaling pathway and mTOR inhibitors in cancer: progress and challenges. Cell & bioscience. 2020;10(1):31.
39. Chen X, Cui Y, Ma Y. Long non-coding RNA BLACAT1 expedites osteosarcoma cell proliferation, migration and invasion via up-regulating SOX12 through miR-608. Journal of Bone Oncology. 2020;25:100314.
40. Malla R, Marni R, Chakraborty A. Exploring the role of CD151 in the tumor immune microenvironment: therapeutic and clinical perspectives. Biochimica et Biophysica Acta (BBA)-Reviews on Cancer. 2023;1878(3):188898.
41. Yang J, Wang L, Guan X, Qin J-J. Inhibiting STAT3 signaling pathway by natural products for cancer prevention and therapy: In vitro and in vivo activity and mechanisms of action. Pharmacological Research. 2022;182:106357.
42. Zhang W, Gong M, Zhang W, Mo J, Zhang S, Zhu Z, et al. Thiostrepton induces ferroptosis in pancreatic cancer cells through STAT3/GPX4 signalling. Cell Death & Disease. 2022;13(7):630.
43. Li S, Huang Y. Ferroptosis: an iron-dependent cell death form linking metabolism, diseases, immune cell and targeted therapy. Clinical and Translational Oncology. 2022;24(1):1-12.
44. Li X, Liu J. FANCD2 inhibits ferroptosis by regulating the JAK2/STAT3 pathway in osteosarcoma. BMC cancer. 2023;23(1):179.
45. Lv H-h, Zhen C-x, Liu J-y, Shang P. PEITC triggers multiple forms of cell death by GSH-iron-ROS regulation in K7M2 murine osteosarcoma cells. Acta Pharmacologica Sinica. 2020;41(8):1119-32.
46. Wen R-j, Dong X, Zhuang H-w, Pang F-x, Ding S-c, Li N, et al. Baicalin induces ferroptosis in osteosarcomas through a novel Nrf2/xCT/GPX4 regulatory axis. Phytomedicine. 2023;116:154881.
47. Stockwell BR, Friedmann Angeli JP, Bayir H, Bush AI, Conrad M, Dixon SJ, et al. Ferroptosis: A Regulated Cell Death Nexus Linking Metabolism, Redox Biology, and Disease. Cell. 2017;171(2):273-85.
48. Marais AD. Apolipoprotein E in lipoprotein metabolism, health and cardiovascular disease. Pathology. 2019;51(2):165-76.
49. Huang Y, Liu XQ, Rall SC, Jr., Taylor JM, von Eckardstein A, Assmann G, et al. Overexpression and Accumulation of Apolipoprotein E as a Cause of Hypertriglyceridemia *. Journal of Biological Chemistry. 1998;273(41):26388-93.
50. Ma HQ, Cui LH, Li CC, Yu Z, Piao JM. Effects of Serum Triglycerides on Prostate Cancer and Breast Cancer Risk: A Meta-Analysis of Prospective Studies. Nutrition and

cancer. 2016;68(7):1073-82.
51. Wan Y, Zhang J, Chen M, Ma M, Sheng B. Elevated serum triglyceride levels may be a key independent predicting factor for gallbladder cancer risk in gallbladder stone disease patients: a case-control study. BMC endocrine disorders. 2022;22(1):270.
52. Broadfield LA, Pane AA, Talebi A, Swinnen JV, Fendt SM. Lipid metabolism in cancer: New perspectives and emerging mechanisms. Developmental cell. 2021;56(10):1363-93.
53. Kemp SB, Carpenter ES, Steele NG, Donahue KL, Nwosu ZC, Pacheco A, et al. Apolipoprotein E Promotes Immune Suppression in Pancreatic Cancer through NF-κB-Mediated Production of CXCL1. Cancer research. 2021;81(16):4305-18.
54. Sohn HY, Kim SI, Park JY, Park SH, Koh YH, Kim J, et al. ApoE4 attenuates autophagy via Fox03a repression in the brain. Scientific reports. 2021;11(1):17604.
55. Parcon PA, Balasubramaniam M, Ayyadevara S, Jones RA, Liu L, Shmookler Reis RJ, et al. Apolipoprotein E4 inhibits autophagy gene products through direct, specific binding to CLEAR motifs. Alzheimer's & dementia : the journal of the Alzheimer's Association. 2018;14(2):230-42.

Figure legends

Figure 1. WGCNA of samples from OS and control groups.

(A) Analysis of network topology for soft threshold power. The figure above shows the scale-free topology model fit. The horizontal red line indicates the chosen cutoff of 0.85 for the scale-free topological fit index. The bottom figure shows the average connectivity as a function of soft-threshold power. (B) Sample dendrogram and trait heatmap. The upper panel is hierarchical clustering dendrogram of the samples based on the expression data, the bottom panel indicates the classification of samples into OS and Control groups. (C) Clustered dendrogram of genes. Different colors represent different gene modules. (D) The eigengene dendrogram and eigengene adjacency heatmap. Colors represent the adjacency between module eigengenes, with red indicating high adjacency and blue indicating low adjacency. (E) Heatmap of the module-trait relationships. The values in the cells represent the correlation coefficients and the corresponding *p*-values in parentheses. WGCNA: Weighted correlation network analysis, OS: Osteosarcoma.

Figure 2. Identification of key OS-related genes and determination of hub gene.

(A) Volcano plot represents DEGs identified from GSE28424. Each point on the graph

corresponds to a gene, with red representing down-regulated genes and yellow representing up-regulated genes. (B) Venn diagram of intersection analysis of 1367 DEGs in the GSE28424 dataset and 99 purple module genes. The overlapping part in the middle is the intersection genes. (C-E) PPI network analysis of 56 intersection genes using MCC (C), MNC (D) and Degree (E) algorithms. Each dot represents the top ten genes of the algorithm, and each line represents the association between genes. (F) Venn diagram, the intersection region of three different network centers, MCC, MNC and Degree, showed nine intersection genes. (G) Box plot of the expression of 9 intersection genes in the GSE28424 dataset in the control and tumor samples. DEGs: differentially expressed genes, PPI: Protein-Protein Interaction, MCC: Maximum Correlation Criterion, MNC: Maximum Neighborhood Component, OS: Osteosarcoma.

Figure 3. Overexpression of *APOE* inhibits proliferation, migration and invasion in OS cells.

(A) qRT-PCR detection of *APOE* mRNA expression in 143B, SW1353, MG-63, SaOS-2, U2OS and HOB cells. (B) WB detection of APOE protein expression in 143B, SW1353, MG-63, SaOS-2, U2OS and HOB cells. (C) Quantitative analysis of APOE protein. (D) qRT-PCR detection of *APOE* overexpression efficiency in 143B and U2OS cell lines. (E) WB detection of APOE overexpression efficiency in 143B and U2OS cell lines. (F) Quantitative analysis of APOE protein. (G and H) CCK-8 detects the cell proliferation of 143B (G) and U2OS (H) on days 0-5 after overexpressing *APOE*. The X-axis is time (days), and the Y-axis is the OD value when the absorbance is 450nm. (I and J) Transwell detection of the invasion and migration abilities of 143B (I) and U2OS (J) after *APOE* overexpression. Scale bar: 50 μm. *p<0.05, **p<0.01, ***p<0.001. qRT-PCR: Quantitative real-time reverse transcription PCR, WB: Western blot, CCK-8: Cell counting kit-8, OD: optical density, OS: Osteosarcoma.

Figure 4. *APOE* overexpression affects the migration and invasion of OS cells mediated by autophagy.

(A and B) Transwell assay for invasion and migration of 143B (A) and U2OS (B) cells,

including Vector, over-*APOE*, Vector+3-MA and over-*APOE*+3-MA groups. Scale bar: 50 μm. (C and D) qRT-PCR detection of *E-cadherin*, *N-cadherin* and *Vimentin* mRNA expression in 143B (C) and U2OS (D) cells, including Vector, over-*APOE*, Vector+3-MA and over-*APOE*+3-MA groups. (E and F) WB detection of E-cadherin, N-cadherin and Vimentin protein expression in 143B (E) and U2OS (F) cells, including Vector, over-*APOE*, Vector+3-MA and over-*APOE*+3-MA groups. (G and H) Quantitative analysis of E-cadherin, N-cadherin and Vimentin. *p<0.05, **p<0.01 vs. Vector, $^{\#}p$<0.05, $^{\#\#}p$<0.01 vs. Over-APOE. qRT-PCR: Quantitative real-time reverse transcription PCR, WB: Western blot, OS: Osteosarcoma.

Figure 5. Overexpression of *APOE* stimulates autophagy in OS cells via the mTOR/Stat3 signaling pathway.

(A) WB detection of p-mTOR and mTOR expression in 143B and U2OS cells overexpressing APOE. (B and C) Quantitative analysis of p-mTOR and mTOR. (D) WB detection of p-Stat3 and Stat3 expression in 143B and U2OS cells overexpressing APOE. (E and F) Quantitative analysis of p-Stat3 and Stat3. (G and H) qRT-PCR detection of *p62*, *LC3B-1*, *LC3B-2* and *Beclin1* expression in 143B and U2OS cells overexpressing *APOE*. (I) WB detection of p62, LC3B-1, LC3B-2, and Beclin1 expression in 143B and U2OS cells overexpressing *APOE*. (J and K) Quantitative analysis of p62, LC3B-1, LC3B-2 and Beclin1. *p<0.05, **p<0.01, ***p<0.001. qRT-PCR: Quantitative real-time reverse transcription PCR, WB: Western blot, OS: Osteosarcoma.

Figure 6. Overexpression of *APOE* induces ferroptosis of OS cells.

(A and B) Detection of apoptosis in 143B (A) and U2OS (B) cells after overexpression of *APOE* by flow cytometry. (C) Relative ROS levels in 143B and U2OS cells transfected with over-*APOE*. (D) Relative Fe^{2+} levels in 143B and U2OS cells transfected with over-*APOE*. (E) Relative SOD levels in 143B and U2OS cells transfected with over-*APOE*. (F) Relative MDA levels in 143B and U2OS cells transfected with over-*APOE*. (G) Relative GSH levels in 143B and U2OS cells

transfected with over-*APOE*. *p<0.05. ROS: Reactive oxygen species, SOD: Superoxide dismutase. MDA: Malondialdehyde, GSH: Glutathione, OS: Osteosarcoma.

Figure 7. Overexpression of *APOE* alters iron metabolism in OS cells.

(A) Relative total iron levels in 143B and U2OS cells transfected with over-*APOE*. (B and C) qRT-PCR detection of *TfR1*, *FPN*, *GPX4* and *SLC7A11* expression in 143B and U2OS cells overexpressing *APOE*. (D) WB detection of TfR1, FPN, GPX4 and SLC7A11 expression in 143B and U2OS cells overexpressing APOE. (E and F) Quantitative analysis of TfR1, FPN, GPX4 and SLC7A11. *p<0.05, **p<0.01, ***p<0.001. qRT-PCR: Quantitative real-time reverse transcription PCR, WB: Western blot, OS: Osteosarcoma.

Figure 8. *APOE* overexpression reduces tumor growth and modulates ferroptosis-related markers in a mouse xenograft model.

(A) Xenograft tumor imaging after nude mice were injected with 143B cells stably transfected with Vector/over-*APOE*. (B) Comparison of tumor weight between Vector and over-*APOE* groups. (C and D) qRT-PCR analysis of mRNA expression levels of autophagy and ferroptosis-related markers, including *LC3B-1*, *LC3B-2*, *GPX4*, *SLC7A11*, *TfR1*, and *FPN* in tumor tissues. (E) WB detection of LC3B-1, LC3B-2, GPX4, SLC7A11, TfR1 and FPN expression in tumor tissues overexpressing *APOE*. (F and G) Quantitative analysis of LC3B-1, LC3B-2, GPX4, SLC7A11, TfR1 and FPN. *p<0.05, **p<0.01, ***p<0.001. OS: Osteosarcoma, qRT-PCR: Quantitative real-time reverse transcription PCR, WB: Western blot.

Supplementary Figure 1. Overexpression of *APOE* induces cell ferroptosis.

Diagram of the mechanism by which *APOE* mediates ferroptosis in OS cells. Overexpression of *APOE* leads to the activation of the mTOR/Stat3 signaling pathway and enhances autophagy, which together suppress OS cell proliferation, migration, and invasion. Additionally, *APOE* overexpression alters iron metabolism, increasing intracellular iron levels, reducing GSH levels, and promoting lipid ROS accumulation.

These changes culminate in the induction of ferroptosis, a form of programmed cell death characterized by iron-dependent lipid peroxidation, thereby contributing to tumor suppression in OS cells. GSH: Glutathione, OS: Osteosarcoma.

Table 1. Primer sequences for *in vitro* qRT-PCR.

Target	Direction	Sequence (5’-3’)
APOE	Forward	TTCCCCAGGAGCCGACTG
APOE	Reverse	ATCCCAAAAGCGACCCAGTG
N-cadherin	Forward	TGGGAAATGGAAACTTGATGGC
N-cadherin	Reverse	AATCTGCAGGCTCACTGCTC
E-cadherin	Forward	GCTGGACCGAGAGAGTTTCC
E-cadherin	Reverse	CAAAATCCAAGCCCGTGGTG
Vimentin	Forward	GGACCAGCTAACCAACGACA
Vimentin	Reverse	AAGGTCAAGACGTGCCAGAG
Beclin 1	Forward	GGGCTCCCGAGGGATGG
Beclin 1	Reverse	TCCTGGGTCTCTCCTGGTTT
LC3B-1	Forward	TCAGGTTCACAAAACCCGCC
LC3B-1	Reverse	CCGTTTACCCTGCGTTTGTG
LC3B-2	Forward	TCAGGTTCACAAAACCCGCC
LC3B-2	Reverse	CCGTTTACCCTGCGTTTGTG
P62	Forward	CATTGCGGAGCCTCATCTCC
P62	Reverse	TCCTCGTCACTGGAAAAGGC
TfR1	Forward	AGCGTCGGGATATCGGGT
TfR1	Reverse	CCATCTACTTGCCGAGCCA
FPN	Forward	AAATCCCTGGGCCCCTTTTC
FPN	Reverse	GGTCATGACACTAGGCGACC
GPX4	Forward	GAGATCAAAGAGTTCGCCGC

GPX4	Reverse	GAACTGTGGAGAGACGGTGT
SLC7A11	Forward	CGCTGTGAAGGAAAAAGCAC
SLC7A11	Reverse	GATGGTGGACACAACAGGCT
GAPDH	Forward	CATGTTGCAACCGGGAAGGA
GAPDH	Reverse	ATCACCCGGAGGAGAAATCG

924

925 **Table 2. Primer sequences for *in vivo* qRT-PCR.**

LC3B-1	Forward	GGGACCCTAACCCCATAGGA
LC3B-1	Reverse	GGCACCAGGAACTTGGTCTT
LC3B-2	Forward	GGGACCCTAACCCCATAGGA
LC3B-2	Reverse	GGCACCAGGAACTTGGTCTT
GPX4	Forward	GCCAAAGTCCTAGGAAACGCC
GPX4	Reverse	CAGGAACTCGGAGCTGTTGC
SLC7A11	Forward	CTGCAGCTAACTGACTGCCC
SLC7A11	Reverse	CCCCTTTGCTATCACCGACT
TfR1	Forward	TAGGCCGCGGGTTCG
TfR1	Reverse	CCGGGTGTATGACAATGGTTC
FPN	Forward	CTCCAACCCGCTCCCATAA
FPN	Reverse	GCACAACAGCCTTATGCCG
GAPDH	Forward	CCCTTAAGAGGGATGCTGCC
GAPDH	Reverse	ATGAAGGGGTCGTTGATGGC

926

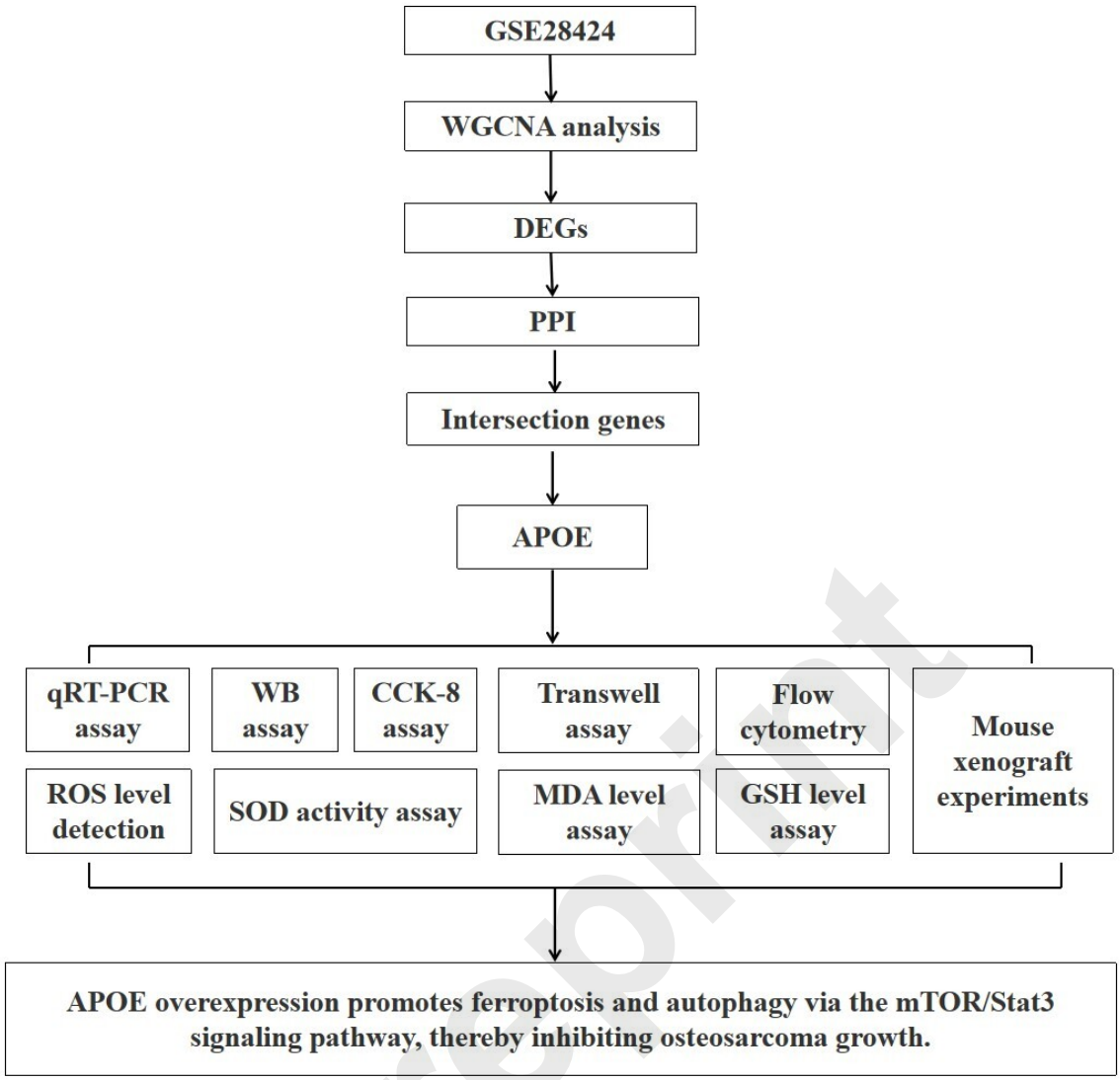
GSE28424
WGCNA analysis
DEGs
PPI
Intersection genes
APOE
qRT-PCR assay
WB assay
CCK-8 assay
Transwell assay
Flow cytometry
Mouse xenograft experiments
ROS level detection
SOD activity assay
MDA level assay
GSH level assay
APOE overexpression promotes ferroptosis and autophagy via the mTOR/Stat3 signaling pathway, thereby inhibiting osteosarcoma growth.

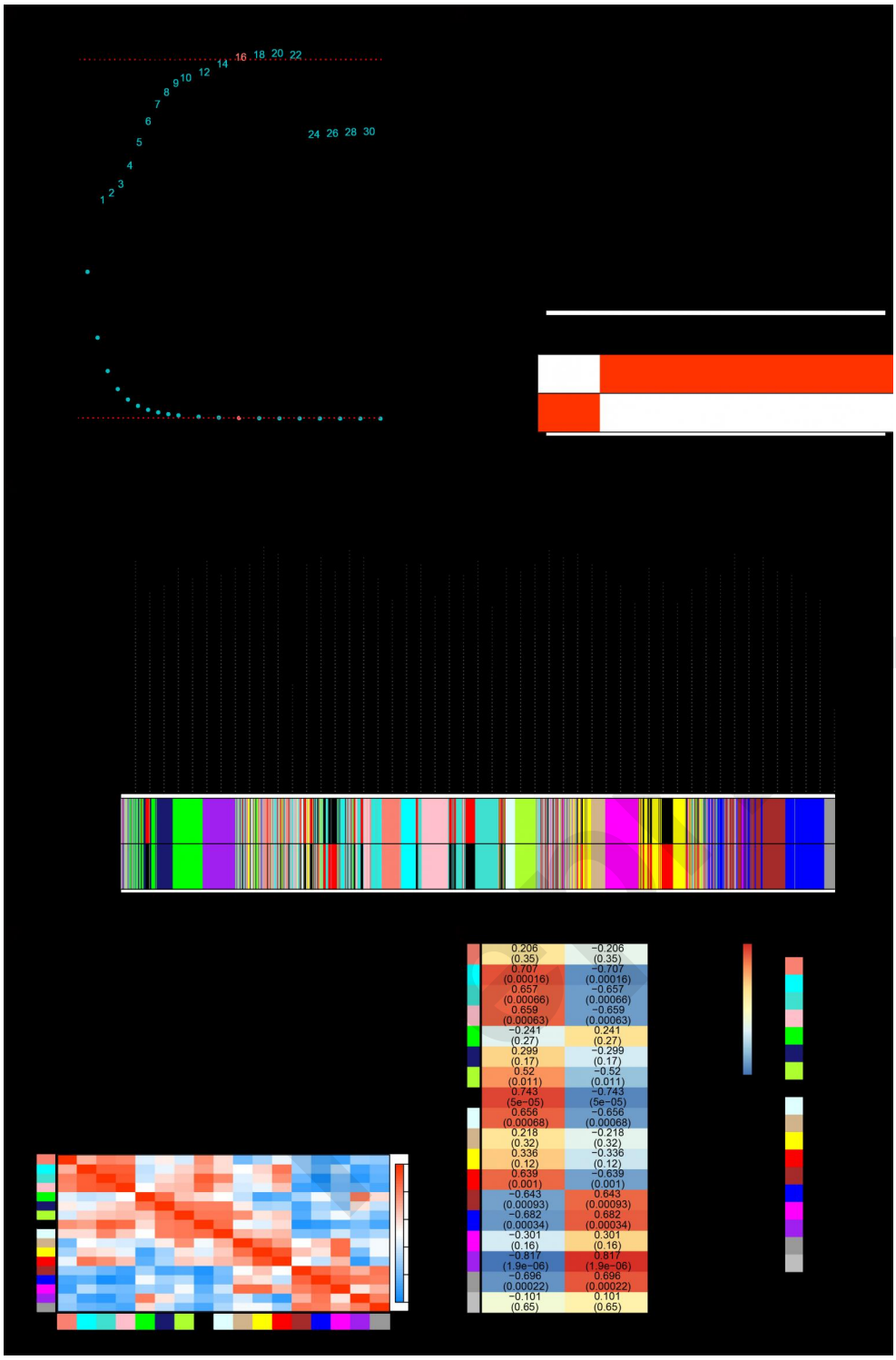
1 2 3 4 5 6 7 8 9 10 12 14 16 18 20 22 24 26 28 30
0.206 (0.35)
−0.206 (0.35)
0.707 (0.00016)
−0.707 (0.00016)
0.657 (0.00066)
−0.657 (0.00066)
0.659 (0.00063)
−0.659 (0.00063)
−0.241 (0.27)
0.241 (0.27)
0.299 (0.17)
−0.299 (0.17)
0.52 (0.011)
−0.52 (0.011)
0.743 (5e−05)
−0.743 (5e−05)
0.656 (0.00068)
−0.656 (0.00068)
0.218 (0.32)
−0.218 (0.32)
0.336 (0.12)
−0.336 (0.12)
0.639 (0.001)
−0.639 (0.001)
−0.643 (0.00093)
0.643 (0.00093)
−0.682 (0.00034)
0.682 (0.00034)
−0.301 (0.16)
0.301 (0.16)
−0.817 (1.9e−06)
0.817 (1.9e−06)
−0.696 (0.00022)
0.696 (0.00022)
−0.101 (0.65)
0.101 (0.65)

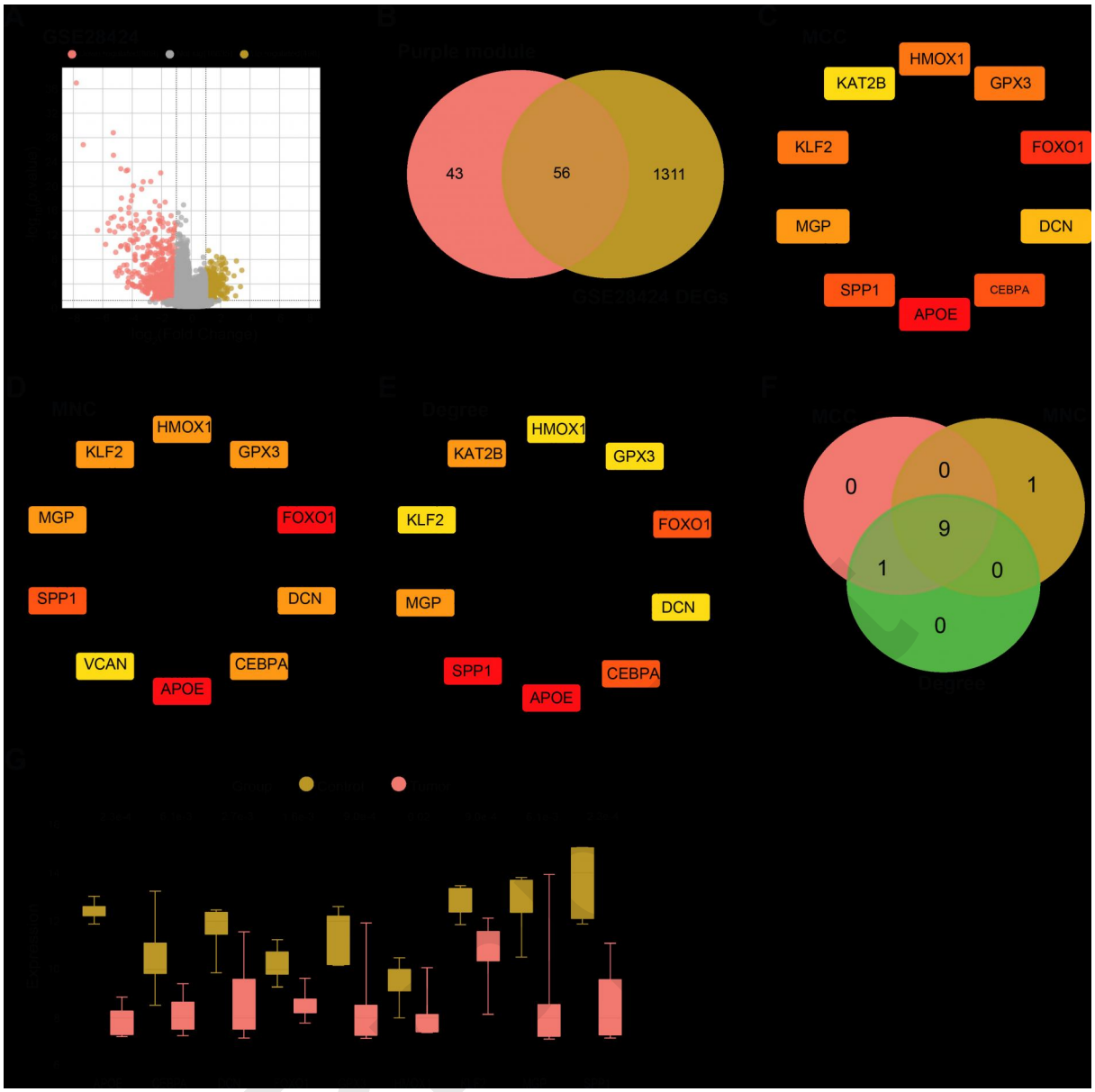
A
GSE28424
Log (Fold Change)
B
Purple module
43
56
1311
GSE28424 DEGs
C
MCC
HMOX1
KAT2B
GPX3
KLF2
FOXO1
MGP
DCN
SPP1
CEBPA
APOE
D
MNC
HMOX1
KLF2
GPX3
MGP
FOXO1
SPP1
DCN
VCAN
CEBPA
APOE
E
Degree
HMOX1
KAT2B
GPX3
KLF2
FOXO1
MGP
DCN
SPP1
CEBPA
APOE
F
MCC
MNC
0
0
1
9
1
0
0
Degree
G
Group
Control
Tumor

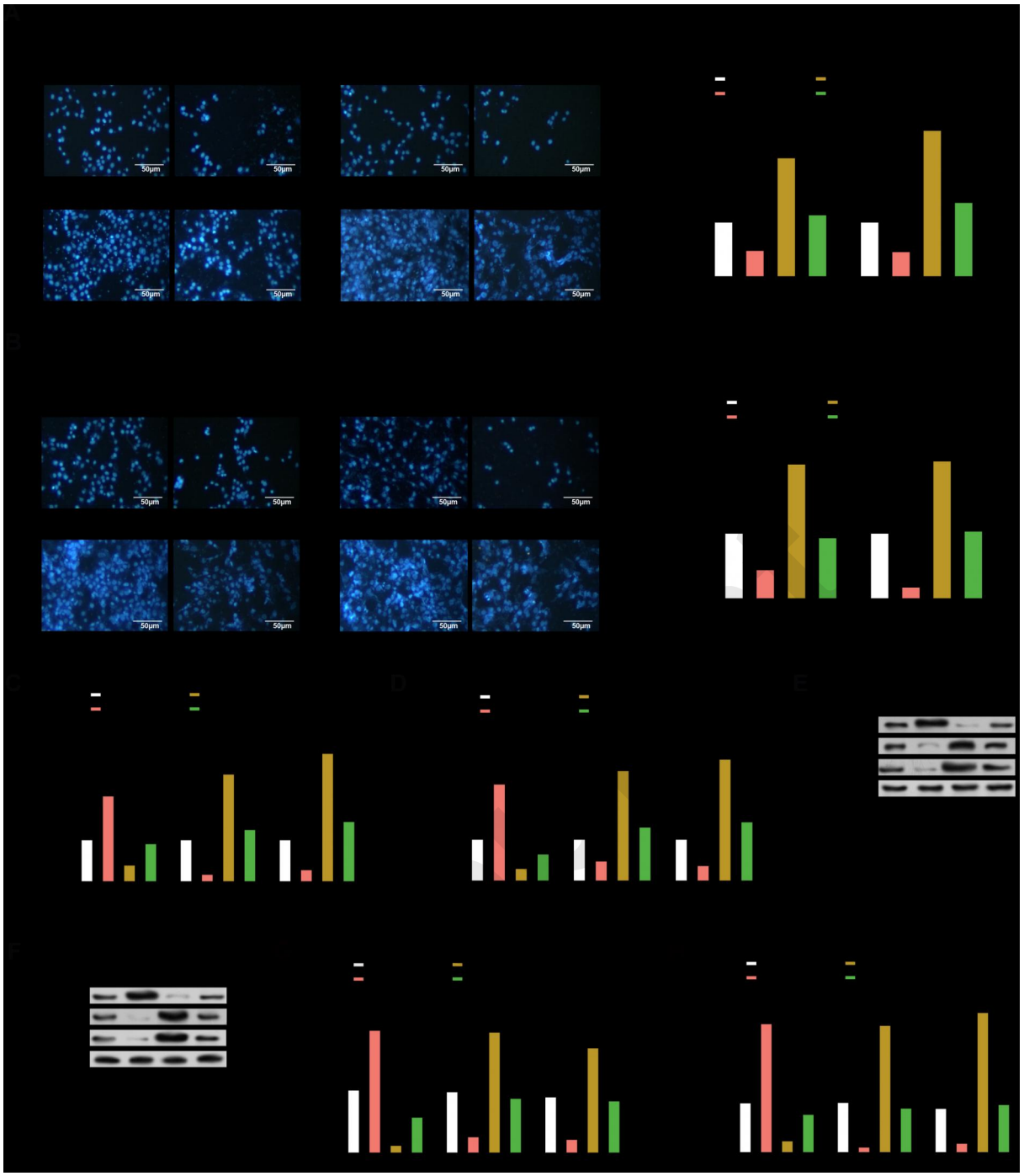
50μm
50μm
50μm
50μm
50μm
50μm
50μm
50μm
50μm
50μm
50μm
50μm
50μm
50μm
50μm
50μm

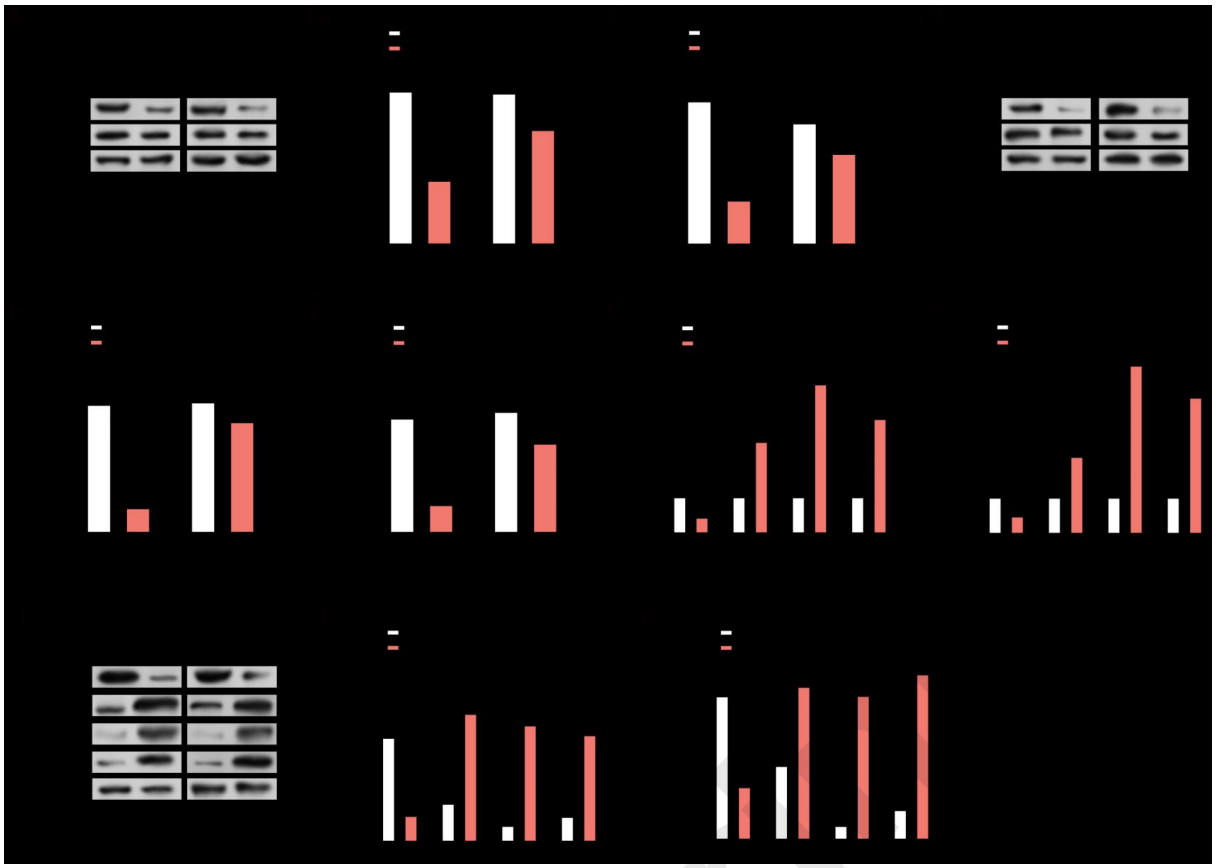

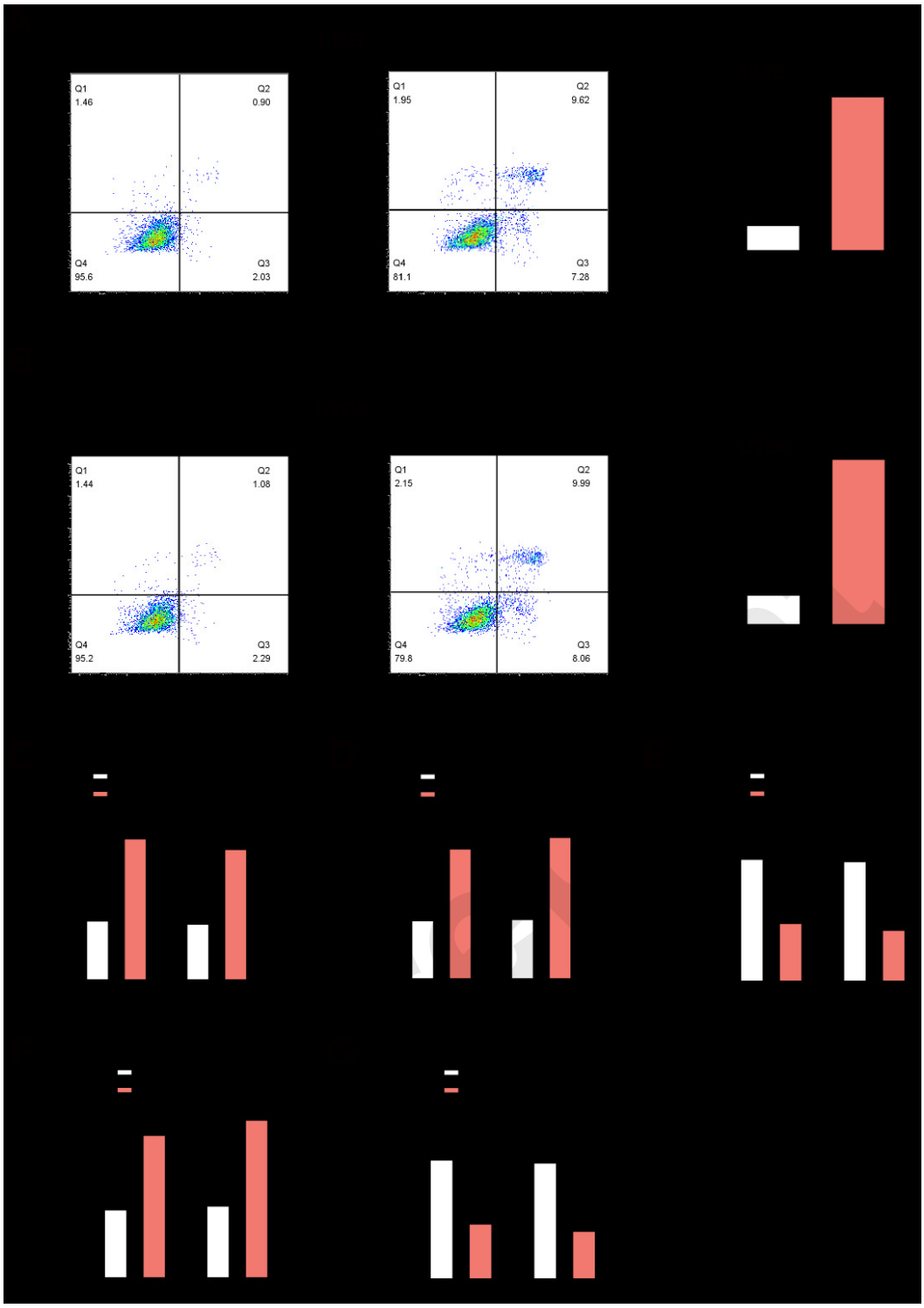
Q1
1.46
Q2
0.90
Q4
95.6
Q3
2.03
Q1
1.95
Q2
9.62
Q4
81.1
Q3
7.28
Q1
1.44
Q2
1.08
Q4
95.2
Q3
2.29
Q1
2.15
Q2
9.99
Q4
79.8
Q3
8.06

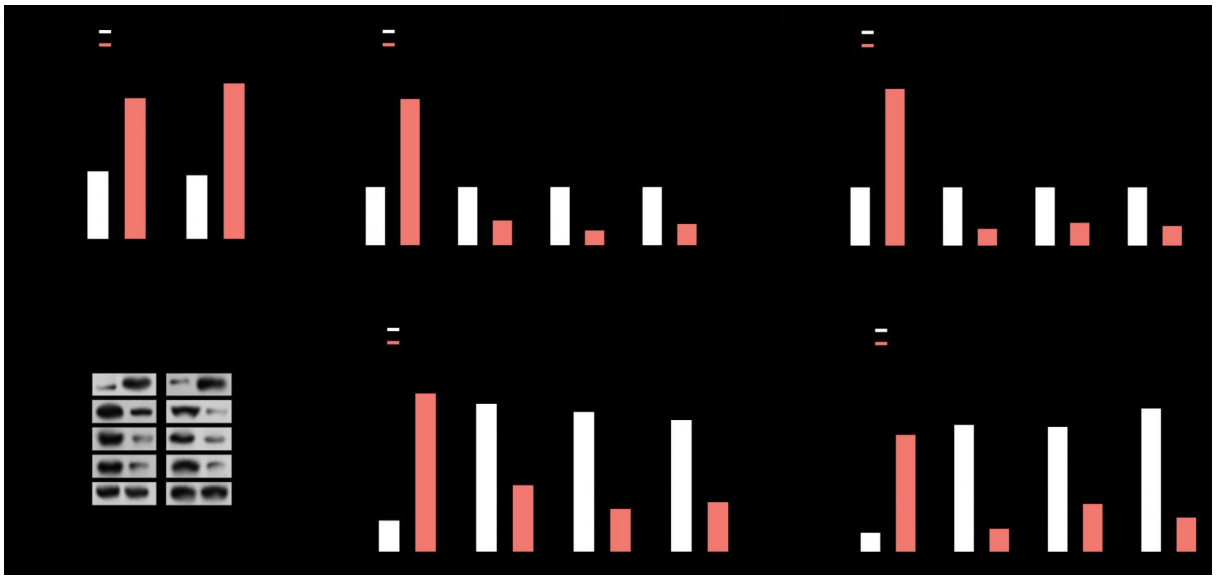

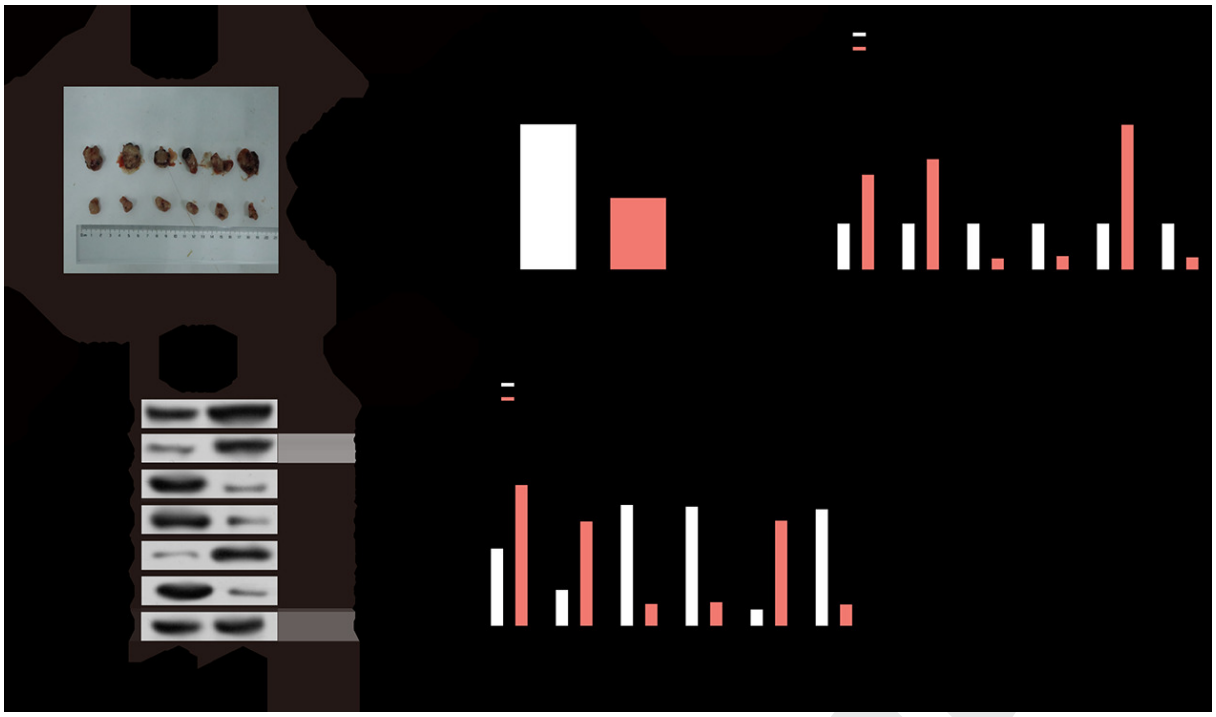

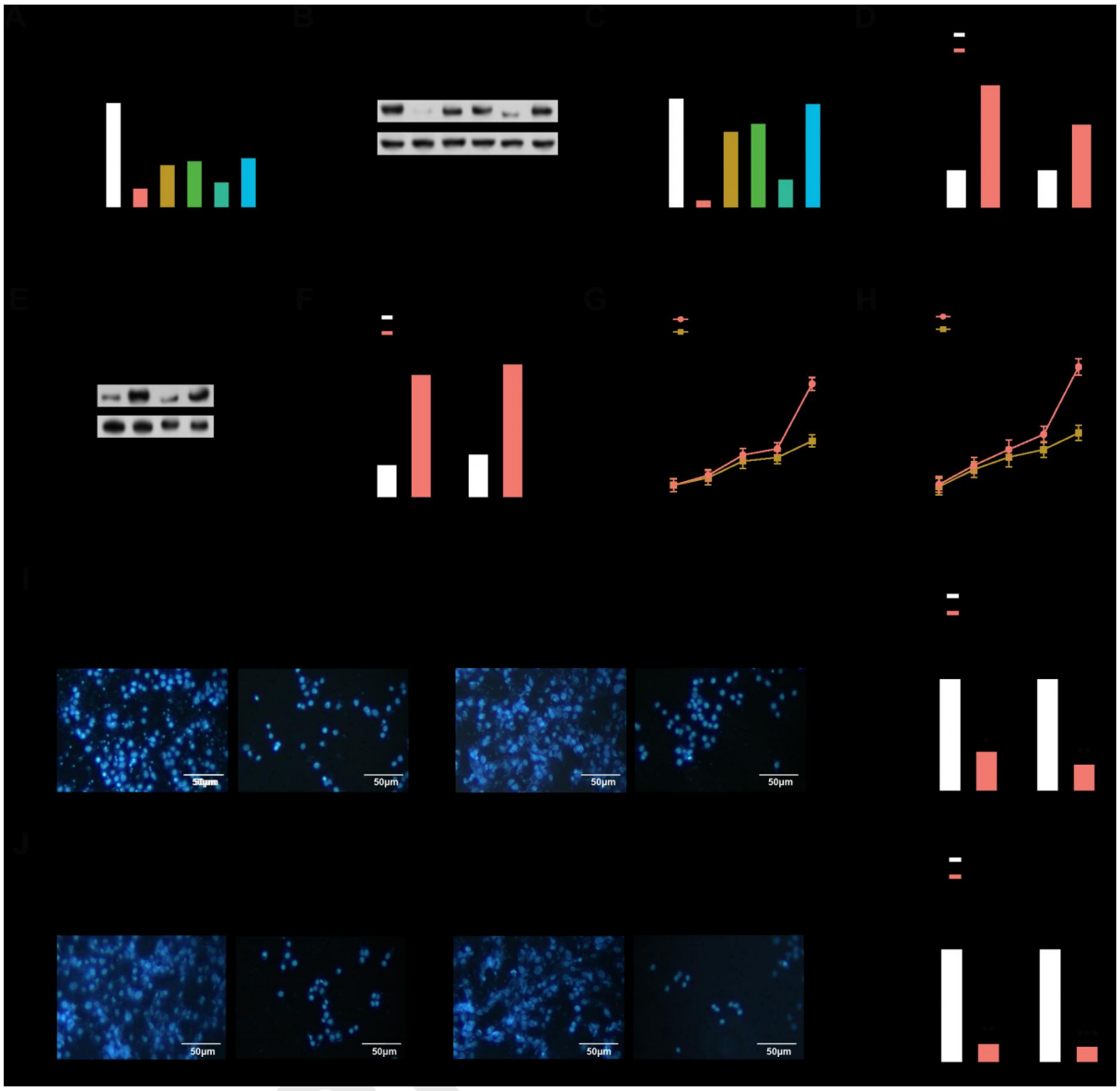
A
B
C
D
E
F
G
H
I
J
50μm
50μm
50μm
50μm
50μm
50μm
50μm
50μm